Heat Transport in Low-Rossby-Number Rayleigh-Bénard Convection

Keith Julien,[1] Edgar Knobloch,[2] Antonio M. Rubio,[1] and Geoffrey M. Vasil[3]

[1]*Department of Applied Mathematics, University of Colorado, Boulder, Colorado 80309, USA*

[2]*Department of Physics, University of California, Berkeley, California 94720, USA*

[3]*Canadian Institute for Theoretical Astrophysics, University of Toronto, 60 St. George Street, Toronto, Ontario, Canada M5S 3H8*

(Received 16 August 2012; revised manuscript received 17 October 2012; published 21 December 2012)

We demonstrate, via simulations of asymptotically reduced equations describing rotationally constrained Rayleigh-Bénard convection, that the efficiency of turbulent motion in the fluid bulk limits overall heat transport and determines the scaling of the nondimensional Nusselt number Nu with the Rayleigh number Ra, the Ekman number E, and the Prandtl number σ. For $E \ll 1$ inviscid scaling theory predicts and simulations confirm the large Ra scaling law $\mathrm{Nu} - 1 \approx C_1 \sigma^{-1/2} \mathrm{Ra}^{3/2} E^2$, where C_1 is a constant, estimated as $C_1 \approx 0.04 \pm 0.0025$. In contrast, the corresponding result for nonrotating convection, $\mathrm{Nu} - 1 \approx C_2 \mathrm{Ra}^{\alpha}$, is determined by the efficiency of the thermal boundary layers (laminar: $0.28 \lesssim \alpha \lesssim 0.31$, turbulent: $\alpha \sim 0.38$). The $3/2$ scaling law breaks down at Rayleigh numbers at which the thermal boundary layer loses rotational constraint, i.e., when the local Rossby number ≈ 1. The breakdown takes place while the bulk Rossby number is still small and results in a gradual transition to the nonrotating scaling law. For low Ekman numbers the location of this transition is independent of the mechanical boundary conditions.

DOI: 10.1103/PhysRevLett.109.254503 PACS numbers: 47.32.Ef, 47.55.pb, 47.27.−i

Introduction.—Rapidly rotating convection is common in stars and planets, and is present in the Earth's oceans and liquid metal core. Such systems remain beyond the reach of laboratory experiment and direct numerical simulation (DNS). Rotating Rayleigh-Bénard convection (RBC) affords an excellent model for studying rotationally influenced buoyancy-driven flow. In RBC, fluid is confined between parallel horizontal plates a distance H apart, rotating rigidly about the vertical with constant angular velocity Ω. Convection is driven by a fixed destabilizing temperature difference ΔT. Three nondimensional control parameters specify the system: the Rayleigh, Ekman, and Prandtl numbers, defined by

$$\mathrm{Ra} \equiv \frac{g\alpha_T \Delta T H^3}{\nu\kappa}, \qquad E \equiv \frac{\nu}{2\Omega H^2}, \qquad \sigma \equiv \frac{\nu}{\kappa}.$$

Here ν is the kinematic viscosity, κ is the thermal diffusivity, g is the gravitational acceleration, and α_T is the thermal expansion coefficient. The Rayleigh number provides a dimensionless measure of the thermal forcing, while the Ekman number measures the importance of viscosity relative to rotation. The convective Rossby number $\mathrm{Ro} \equiv E\sqrt{\mathrm{Ra}/\sigma} = \sqrt{g\alpha_T \Delta T/4H\Omega^2}$ thus measures the importance of thermal forcing relative to rotation. Rotationally constrained systems are characterized by $\mathrm{Ro} \ll 1$.

Understanding the scaling dependence of global fluid properties on the independent parameters $\{\mathrm{Ra}, E, \sigma\}$ is critical for identifying regime transitions and potential extrapolation to natural environments. An important quantity in this regard is the global heat transport as measured by the Nusselt number $\mathrm{Nu} \equiv qH/\rho_0 c_p \kappa \Delta T$, where q is the total heat flux and $\rho_0 c_p$ is the volumetric heat capacity. At large Ra the convective scaling law in a given flow regime assumes the general form

$$\mathrm{Nu} - 1 \approx C(\sigma)\mathrm{Ra}^{\alpha} E^{\beta}, \tag{1}$$

where the exponents α and β measure the marginal convective heat transport (efficiency) with respect to differential increases in Ra and E. In general, the values of α, β, C lack universality and take different values in different parameter regimes, indicating changes in the dominant underlying physics.

In nonrotating or rotationally unconstrained convection ($\mathrm{Ro} \gg 1$), Nu is independent of E, and hence $\beta \approx 0$. The determination of the remaining exponent α has a long history. The theory of Malkus [1] rests on the premise that a thin laminar thermal boundary layer with temperature drop $\Delta T/2$ remains marginally stable and launches plumes into a well-mixed deep interior. In this model the heat flux, $q = \mathrm{Nu}\rho_0 c_p \kappa \Delta T/H$, is independent of H, and hence $\alpha \approx 1/3$ [1,2]. A more comprehensive model introduced recently by Grossmann and Lohse [3] yielded $0.28 \lesssim \alpha \lesssim 0.31$, in excellent agreement with modern experiments [4,5]. When the shear across the viscous boundary layers at the top and bottom due to the turbulent flow in the interior becomes sufficiently large, these layers become themselves turbulent resulting in $\alpha = 1/2$ [6], albeit with logarithmic corrections owing to the development of a thermal sublayer which acts to *throttle* heat transport and yields an effective exponent close to 0.38 [6,7].

When $\mathrm{Ro} \ll 1$, geostrophic balance and the Taylor-Proudman effect [8] favor invariance along the rotation axis thereby suppressing global heat transport relative to nonrotating RBC. In particular, the mean temperature gradient in the layer midplane saturates as Ra increases [9,10], in contrast to nonrotating RBC where it becomes small or vanishes as Ra increases [11,12]. The temperature drop across the thermal boundary layers at the top and bottom is therefore smaller than in nonrotating RBC and their structure differs [10]. As we show below, this results in heat transport that is throttled in the bulk instead of the thermal boundary layers, although the exponent is in fact larger: $\alpha > 1$.

Some debate exists in the literature over the evidence for a low-Ro scaling law when Ra is well beyond critical (but Ro $\ll 1$). Experiments [7,13–17] barely extend into the low Ro regime and suggest that $1 \lesssim \alpha \lesssim 3$ for the explored range $10^{-6} \leq E$, $10^3 \leq \mathrm{Ra} \leq 10^9$. Based on DNS with no-slip boundaries, King *et al.* [18] argue in favor of depth-independent heat flux as in the approach of Malkus [1] and propose the scaling exponents $\alpha = 3$, $\beta = 4$ so that $\mathrm{Ra}^3 E^4 \sim H$. In contrast, stress-free boundaries yield distinctly different exponents, $(\alpha, \beta) \approx (6/5, 8/5)$ [19].

Linear stability theory for rotating RBC with both stress-free and no-slip boundaries shows that in the limit of strong rotation ($E \rightarrow 0$) the critical Rayleigh number Ra_c for the onset of convection increases according to $\mathrm{Ra}_c \propto E^{-4/3}$ [20]. Since for $\mathrm{Ra}_c \ll \mathrm{Ra} \lesssim \mathrm{Ra}_t$ (see below) Nu is expected to depend only on $\mathrm{Ra}/\mathrm{Ra}_c$, it follows that $\beta = 4\alpha/3$ and hence that Eq. (1) becomes $\mathrm{Nu} - 1 \propto (\mathrm{Ra}E^{4/3})^{\alpha}$. However, in the no-slip case rotationally constrained asymptotic scaling laws may not set in until $E \lesssim 10^{-6}$ [21]. Such values of E have not been realized in experiments and DNS while simultaneously increasing $\mathrm{Ra}E^{4/3}$ sufficiently to probe strong geostrophic turbulence. As a result the parameter range explored to date typically captures coherent dynamics involving convective Taylor columns (CTCs) [9,22] but not geostrophic turbulence. Nevertheless, the recent experiments by King *et al.* [15] undeniably show that the transition away from a rotationally constrained scaling law occurs *entirely within* the low-Ro-regime with the transitional Rossby number $\mathrm{Ro}_t \rightarrow 0$ as $E \rightarrow 0$. The authors propose that the transition occurs when the diminishing width of the thermal boundary layer becomes comparable with the Ekman layer, despite the fact that a similar transition is observed for stress-free boundary conditions and no Ekman layers [19].

In this Letter, we identify a compelling alternative to the $\alpha \approx 3$, $\beta \approx 4$ scaling and propose a mechanism for the above transition by going deeper into the rapid rotation regime. Our results support the suggestion that in rotationally constrained turbulence heat transport is independent of microscopic diffusion coefficients just as in nonrotating turbulence. Together with the requirement $\beta = 4\alpha/3$ this suggestion leads to $\alpha = 3/2$, $\beta = 2$, i.e.,

$$\mathrm{Nu} - 1 \approx C_1 \sigma^{-1/2} \mathrm{Ra}^{3/2} E^2, \tag{2}$$

where C_1 is constant. Our simulations of geostrophic turbulence (Fig. 1) using reduced equations valid in the limit $E \rightarrow 0$ confirm this scaling (Fig. 2) and indicate that $C_1 \approx 1/25$. In contrast to the nonrotating case, the turbulent

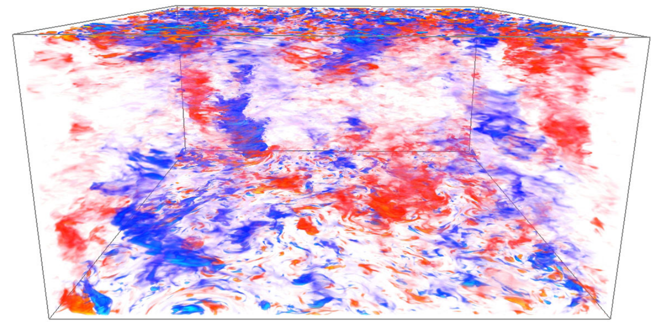

FIG. 1 (color online). Volume rendering of thermal fluctuations θ in the geostrophic turbulence regime for $\mathrm{Ra}E^{4/3} = 160$ and $\sigma = 0.3$.

scaling, Eq. (2), predicts *less* efficient transport than the argument of King *et al.* [18]. This implies that the vertical stiffness of a geostrophically balanced turbulent interior acts as the primary throttling agent on the heat transport, preventing the associated plume-emitting thermal boundary layers and geostrophic vortices from reaching their peak efficiency. Consequently, unlike hypotheses conjectured in Refs. [15,18,19], boundary conditions play no role in determining the scaling exponent α. Below we present evidence for Eq. (2) and give a new analysis of the global heat transport for $E \rightarrow 0$. We also demonstrate that the primary cause of the break in Nu at Ra_t is the loss of geostrophic balance in a dynamically active thermal boundary layer owing to increased vertical mixing, and ultimately a complete loss of rotational constraint. Furthermore, we predict that the transitional {Ra, Ro} values scale as

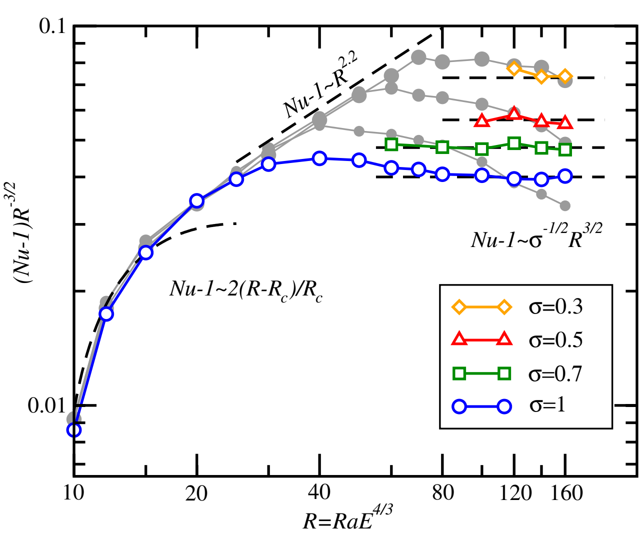

FIG. 2 (color online). $\mathrm{Nu} - 1$ as a function of $R \equiv \mathrm{Ra}E^{4/3}$, compensated with the geostrophic turbulence scaling prediction $R^{3/2}$. The curves for $\sigma \leq 1$ exhibit the predicted scaling for geostrophic turbulence, $\mathrm{Nu} - 1 \propto C_1 \sigma^{-1/2} R^{3/2}$ to within 6%. The $\sigma = 3$, 7 and 15 states, shown as small, medium, and large gray circles, respectively, have yet to reach the turbulent scaling regime.

$$\mathrm{Ra}_t \approx E^{-8/5}, \qquad \mathrm{Ro}_t \approx E^{1/5} \quad \text{as } E \to 0. \tag{3}$$

Theory.—In statistically stationary turbulence Nu represents the sum of the diffusive and convective heat fluxes and is independent of the vertical coordinate z. The scaling with Ra may therefore be determined at any height z, and it is convenient to focus on dynamics above and below the equipartition level $z = \eta$ at which the convective heat flux, dominant in the bulk, is equal to the diffusive heat flux, dominant in the thermal boundary layer. For this purpose we write the velocity field as $\boldsymbol{u} = \boldsymbol{u}_\perp + w\hat{\boldsymbol{z}}$ and the temperature as $T = \bar{T}(z) + \theta$, where $\bar{T}(z)$ is the time-averaged temperature. We nondimensionalize all quantities using the depth H, velocity κ/H, time H^2/κ, and temperature ΔT. In the rapid rotation limit we expect horizontal scales of order $E^{1/3}H$ near onset ($\mathrm{Ra} \sim \mathrm{Ra}_c$) and dynamically similar behavior in the thermal boundary layers and bulk when $\mathrm{Ra} \gg \mathrm{Ra}_c$ [23,24]. For $\mathrm{Ra} \gg \mathrm{Ra}_c$ the appropriate scales for the thermal boundary layer are

$$\boldsymbol{x}_\perp \to \frac{E^{1/3}}{R^\lambda}\boldsymbol{x}'_\perp, \quad z \to \frac{1}{R^{3\lambda}}z', \quad t \to \frac{E^{2/3}}{R^{2\lambda}}t', \tag{4}$$

$$\boldsymbol{u}_\perp \to \frac{R^\lambda}{E^{1/3}}\boldsymbol{u}'_\perp, \quad w \to \frac{R^\lambda}{E^{1/3}}w', \quad p \to \frac{p'}{E}, \tag{5}$$

$$\theta \to E^{1/3}R^{3\lambda-1}\theta', \qquad \partial_z\bar{T} \to R^{4\lambda-1}(\partial_z\bar{T})', \tag{6}$$

where $R \equiv \mathrm{Ra}E^{4/3}$ and $1/3 < \lambda \le 1$ is an arbitrary scaling exponent that determines the vertical scale $\eta \sim R^{-3\lambda}$ of the layer and the temperature drop $\delta\bar{T} \sim \eta\partial_z\bar{T}$ across it. After dropping primes the resulting boundary layer equations take the form

$$\frac{1}{\sigma}\frac{D\boldsymbol{u}_\perp}{Dt} + \frac{\hat{\boldsymbol{z}}\times\boldsymbol{u}_\perp + \boldsymbol{\nabla}_\perp p}{\varepsilon} = (\boldsymbol{\nabla}_\perp^2 + \varepsilon^2\partial_z^2)\boldsymbol{u}_\perp, \tag{7}$$

$$\frac{1}{\sigma}\frac{Dw}{Dt} + \partial_z p = \theta + (\boldsymbol{\nabla}_\perp^2 + \varepsilon^2\partial_z^2)w, \tag{8}$$

$$\boldsymbol{\nabla}_\perp \cdot \boldsymbol{u}_\perp + \varepsilon\partial_z w = 0, \tag{9}$$

$$\frac{D\theta}{Dt} + w\partial_z\bar{T} = (\boldsymbol{\nabla}_\perp^2 + \varepsilon^2\partial_z^2)\theta, \tag{10}$$

$$R^{-4\lambda+1}Nu = \overline{w\theta} - \partial_z\bar{T}, \tag{11}$$

where $\varepsilon \equiv E^{1/3}R^{2\lambda}$ and $D/Dt \equiv \partial_t + \boldsymbol{u}_\perp\cdot\boldsymbol{\nabla}_\perp + \varepsilon w\partial_z$. Five conclusions follow from this rescaling when $\varepsilon \ll 1$:

(A) In order that Nu remains in Eq. (11) as $R \to \infty$, Nu must scale as $\mathrm{Nu} \sim R^{4\lambda-1}$. Comparison with the turbulent scaling, Eq. (2), leads to the prediction $\lambda = 5/8$.

(B) Equation (7) implies that $\boldsymbol{u}_\perp = \hat{\boldsymbol{z}}\times\boldsymbol{\nabla}_\perp p + \varepsilon\boldsymbol{u}_1 + \mathcal{O}(\varepsilon^2)$, representing geostrophic balance at leading order, while Eq. (9) implies that $\boldsymbol{\nabla}_\perp\cdot\boldsymbol{u}_1 + \partial_Z W = \mathcal{O}(\varepsilon)$. Taking the horizontal curl of Eq. (7), and eliminating $\boldsymbol{u}_1$ leads to a closed set of equations describing the dynamics in the thermal boundary layer when $R \gg 1$. The resulting equations are the *same* as those describing the *whole* domain when $R = \mathcal{O}(1)$, i.e., $R \lesssim \mathrm{Ra}_t E^{4/3} = E^{-4/15}$ [23,24], and can be written in the form

$$\frac{1}{\sigma}(\partial_t + \boldsymbol{u}_\perp\cdot\boldsymbol{\nabla}_\perp)\boldsymbol{\nabla}_\perp^2 p - \partial_z w = \boldsymbol{\nabla}_\perp^4 p + \mathcal{O}(\varepsilon), \tag{12}$$

$$\frac{1}{\sigma}(\partial_t + \boldsymbol{u}_\perp\cdot\boldsymbol{\nabla}_\perp)w + \partial_z p = R\theta + \boldsymbol{\nabla}_\perp^2 w + \mathcal{O}(\varepsilon), \tag{13}$$

$$(\partial_t + \boldsymbol{u}_\perp\cdot\boldsymbol{\nabla}_\perp)\theta + w\partial_z\bar{T} = \boldsymbol{\nabla}_\perp^2\theta + \mathcal{O}(\varepsilon). \tag{14}$$

Here $\boldsymbol{u}_\perp = \hat{\boldsymbol{z}}\times\boldsymbol{\nabla}_\perp p$, and $\mathrm{Nu} \equiv \overline{w\theta} - \partial_z\bar{T}$ solves a nonlinear eigenvalue problem specified by the boundary conditions

$$\bar{T}(z=0) = 1, \qquad \bar{T}(z=1) = 0. \tag{15}$$

In the following we refer to Eqs. (12)–(15) as the reduced equations.

(C) Geostrophic balance in the thermal boundary layer breaks down when $\varepsilon \sim 1$, i.e., $E^{1/3}R^{2\lambda} \sim 1$. This condition is equivalent to the statement that the local convective Rossby number in the boundary layer $\mathrm{Ro}_{\mathrm{loc}} \sim E_{\mathrm{loc}}\mathrm{Ra}_{\mathrm{loc}}^{1/2} \sim E^{1/3}R^{2\lambda} \sim 1$. For $\lambda = 5/8$ this occurs when Ra reaches $\mathrm{Ra}_t \approx E^{-8/5}$ as $E \to 0$, or equivalently, when $\mathrm{Ro} = \mathrm{Ro}_t \approx E^{1/5}$ [Eq. (3)]. Thus the transition from rotation-dominated flow ($\varepsilon \ll 1$) to rotation-affected flow ($\varepsilon \gtrsim 1$) in the thermal boundary layers occurs in the regime of strong rotation as measured by the bulk convective Rossby number Ro. These layers are characterized by relative temperature gradient $\partial_z\bar{T} \approx \mathrm{Nu}/2 \sim R^{4\lambda-1}$ and possess local values for Ra and E given by $\mathrm{Ra}_{\mathrm{loc}} = \mathrm{RaNu}\eta^4 \sim E^{-4/3}R^{-8\lambda} = \varepsilon^{-4}$, and $E_{\mathrm{loc}} = E/\eta^2 \sim ER^{6\lambda} = \varepsilon^3$. Thus for any set of values of $\{\lambda, E, R\}$, $R_{\mathrm{loc}} = \mathrm{Ra}_{\mathrm{loc}}E_{\mathrm{loc}}^{4/3} \sim 1$. Given that convection sets in for $R_{\mathrm{loc}} \sim 1$ the self-similar thermal boundary layer is marginally stable as proposed by Malkus.

(D) In the transition regime, the magnitudes of the quantities in Eqs. (4)–(6) become fully isotropic with $|\boldsymbol{\nabla}_\perp| \sim |\partial_z| \sim |\boldsymbol{u}_\perp| \sim |w| \sim E^{-1/2}$ for any λ, while $|\theta| \sim |\delta\bar{T}| \sim E^{(1-\lambda)/6\lambda}$, scalings characterizing moderate-to-nonrotating RBC [25]. In this regime the $\mathcal{O}(\varepsilon)$ terms in Eqs. (7)–(11) play significant dynamic roles, indicating complete loss of geostrophic balance, even though the interior remains rotationally constrained with bulk Ro, $E \ll 1$.

(E) The transitional interval from Eq. (2) to rotationally unaffected scalings ($\mathrm{Ro} \gtrsim 1$) is characterized by enhanced heat transport [13] resulting from Ekman pumping as described by Zhong *et al.* [26]. The width of this interval is $E^{1/5} \lesssim \mathrm{Ro} \lesssim 1$ ($E^{-8/5} \lesssim \mathrm{Ra} \lesssim E^{-2}$).

Simulations.—We integrate Eqs. (12)–(15) for fixed $10 \le R \le 160$ and $\varepsilon \to 0$ until a stationary state is reached (Fig. 1 and Refs. [9,10]). Our most turbulent simulations were well resolved with 768:768:385 spectral modes.

When $\sigma > 0.68$ and R increases beyond $R = R_c \approx 8.7$, we find four distinct regimes, all identifiable by transitions in compensated Nu-Ra plots (Fig. 2) for different σ: (i) a σ-independent laminar cellular state characterized by $\mathrm{Nu} - 1 \approx 2(R - R_c)/R_c$, (ii) a σ-independent state of isolated layer-spanning convective Taylor columns characterized by $\mathrm{Nu} - 1 \sim R^2$ [10], (iii) an intermediate plume state resulting from a σ-dependent disruption of the CTCs that reduces convection efficiency, and ultimately, for $\sigma \leq 1$, (iv) a state of geostrophic turbulence (Fig. 1) at sufficiently large R. The $\mathrm{Nu} - 1 \sim \sigma^{-1/2} R^{3/2}$ scaling expected of regime (iv) is reflected in Fig. 2. Here measurements were taken during the quasistationary state seen after initial transients decay but before an inverse cascade mechanism generates a slowly evolving large-scale barotropic mode as described in Ref. [10]; this interval shrinks as σ decreases. Figures 3(a)–3(c) show the corresponding behavior of rms temperature, vertical vorticity, and vertical velocity fluctuations at the equipartition level. For $\sigma \leq 1$ each shows a transition to geostrophic turbulence as R increases.

Equations (12)–(15) yield a power integral for the thermal dissipation rate $\mathcal{E}_\theta \equiv \langle(\partial_z \bar{T})^2\rangle + \langle|\nabla_\perp \theta|^2\rangle = Nu$, where $\langle\ldots\rangle$ indicates volume and time averages [10].

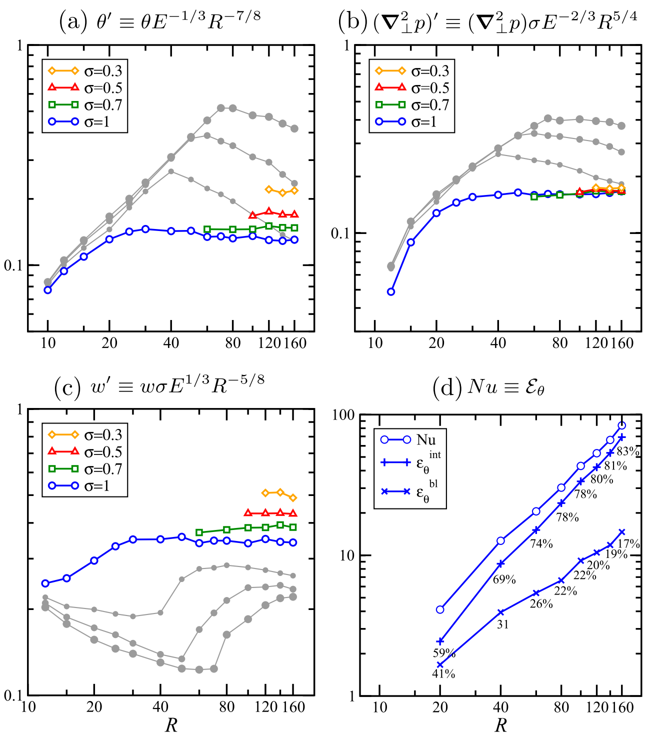

FIG. 3 (color online). (a) Root-mean-square temperature fluctuation θ'_{rms}, (b) rms vertical vorticity $(\nabla_\perp^2 p)'_{\mathrm{rms}}$, (c) rms vertical velocity w'_{rms}, all as a function of $R \equiv \mathrm{Ra}E^{4/3}$ evaluated at $z = \eta$ for different σ. Each nondimensional quantity is scaled according to the geostrophic predictions, Eqs. (4)–(6), with $\lambda = 5/8$. (d) Contributions (in percentage form) to $\mathrm{Nu} \equiv \mathcal{E}_\theta$ measured by the thermal dissipation rate in the interior, $\mathcal{E}_\theta^{\mathrm{int}}$, and the boundary layer, $\mathcal{E}_\theta^{\mathrm{bl}}$, as functions of R when $\sigma = 1$.

Partitioning $\mathcal{E}_\theta$ into interior (bulk) and boundary layer contributions, i.e., $\mathcal{E}_\theta = \mathcal{E}_\theta^{\mathrm{int}} + \mathcal{E}_\theta^{\mathrm{bl}}$, proves useful in identifying regions within the fluid layer that throttle the heat flux [3]. Figure 3(d) shows the energy dissipation rates in the boundary layer $\mathcal{E}_\theta^{\mathrm{bl}}$ and in the bulk $\mathcal{E}_\theta^{\mathrm{int}}$, and reveals that dissipation in the bulk increases with increasing Ra, confirming that it is the bulk that limits the Nusselt number.

In Fig. 4(a) we show the compensated scaling for the thermal boundary layer width η while Fig. 4(b) shows the temperature drop $\delta\bar{T}$ across η. As in Fig. 3 both show solid agreement with predictions based on $\lambda = 5/8$. In particular, $\delta\bar{T}$ does not saturate as R increases ($\delta\bar{T} \sim R^{-3/8}$), in contrast to the assumption made in Refs. [1,18].

Our study of the reduced equations for $R \leq 160$ provides convincing evidence for the presence of geostrophic turbulence when $\sigma \leq 1$. In contrast, for $\sigma \gtrsim 3$ the system remains in the CTC regime with $\alpha \approx 2$. Reduced inertia in Eqs. (12) and (13) as σ increases delays the onset of saturation in all quantities, and hence the transition to geostrophic turbulence. Based on a presumption that $\mathrm{Nu} \propto (R/\sigma^{1/3})^{3/2}$ in the geostrophic turbulence regime, we anticipate threshold values of $R_{\mathrm{turb}} \approx 220$, 290, 370 for $\sigma = 3$, 7, 15, respectively. The shift from $\alpha \approx 2$ to $\alpha \approx 3/2$ (Fig. 2) indicates that it is the turbulent interior that limits the heat flux, in stark contrast to nonrotating RBC.

The results of this Letter characterize the asymptotic state of RBC in the limit $\varepsilon \to 0$. With no-slip boundary conditions this state may not be reached until $\varepsilon \lesssim 10^{-2}$ ($E \lesssim 10^{-6}$), even within linear theory [21]. Thus no-slip DNS at $E \geq 10^{-6}$ finds steeper exponents [18] while stress-free DNS results in shallower exponents [19]. There is a considerable need, therefore, for further detailed DNS and laboratory experiments at $\sigma \leq 1$, $E \leq 10^{-8}$, and $\mathrm{Ra}E^{4/3} \geq 100$, i.e., $\mathrm{Ra} \geq 10^{12}$ ($\sigma = 7$, $E \leq 10^{-10}$, and $\mathrm{Ra}E^{4/3} \geq 400$, i.e., $\mathrm{Ra} \geq 10^{14}$), despite the challenge posed by these parameter values.

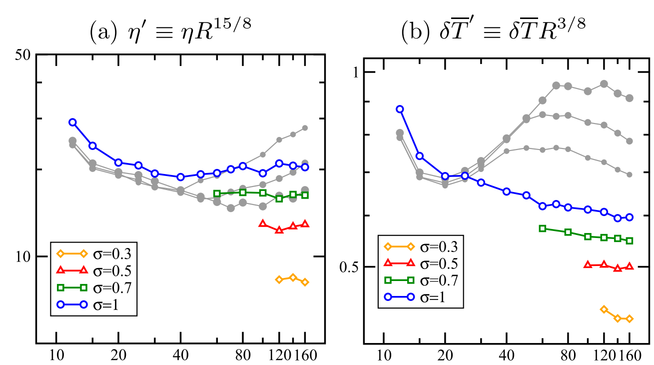

FIG. 4 (color online). Boundary layer quantities as functions of $R \equiv \mathrm{Ra}E^{4/3}$ for different σ. (a) The width η' and (b) the temperature drop $\delta\bar{T}'$. Each nondimensional quantity is scaled according to the geostrophic predictions, Eqs. (4)–(6), with $\lambda = 5/8$.

This work was supported by NSF FRG Grants No. DMS-0855010 and No. DMS-0854841. The authors would like to thank Jon Aurnou, Michael Calkins, and Robert Ecke for useful discussion. All authors contributed equally to this work.

[1] W. V. R. Malkus, Proc. R. Soc. A **225**, 196 (1954).
[2] C. H. B. Priestley, Aust. J. Phys. **7**, 176 (1954).
[3] S. Grossmann and D. Lohse, J. Fluid Mech. **407**, 27 (2000).
[4] X. Xu, K. M. S. Bajaj, and G. Ahlers, Phys. Rev. Lett. **84**, 4357 (2000).
[5] G. Ahlers and X. Xu, Phys. Rev. Lett. **86**, 3320 (2001).
[6] R. H. Kraichnan, Phys. Fluids **5**, 1374 (1962).
[7] G. Ahlers, S. Grossmann, and D. Lohse, Rev. Mod. Phys. **81**, 503 (2009).
[8] G. I. Taylor, Phil. Trans. R. Soc. A **223**, 289 (1923).
[9] M. Sprague, K. Julien, E. Knobloch, and J. Werne, J. Fluid Mech. **551**, 141 (2006).
[10] K. Julien, A. M. Rubio, I. Grooms, and E. Knobloch, Geophys. Astrophys. Fluid Dyn. **106**, 392 (2012).
[11] A. Tilgner, A. Belmonte, and A. Libchaber, Phys. Rev. E **47**, R2253 (1993).
[12] G. Ahlers, E. Bodenschatz, D. Funfschilling, S. Grossmann, X. He, D. Lohse, R. J. A. M. Stevens, and R. Verzicco, Phys. Rev. Lett. **109**, 114501 (2012).
[13] H. T. Rossby, J. Fluid Mech. **36**, 309 (1969).
[14] Y. Liu and R. E. Ecke, Phys. Rev. Lett. **79**, 2257 (1997).
[15] E. King, S. Stellmach, J. Noir, U. Hansen, and J. Aurnou, Nature (London) **457**, 301 (2009).
[16] Y. Liu and R. E. Ecke, Phys. Rev. E **80**, 036314 (2009).
[17] J. Zhong and G. Ahlers, J. Fluid Mech. **665**, 300 (2010).
[18] E. King, S. Stellmach, and J. Aurnou, J. Fluid Mech. **691**, 568 (2012).
[19] S. Schmitz and A. Tilgner, Phys. Rev. E **80**, 015305 (2009).
[20] S. Chandrasekhar, *Hydrodynamic and Hydromagnetic Stability* (Oxford University, New York, 1961).
[21] P. P. Niiler and F. E. Bisshopp, J. Fluid Mech. **22**, 753 (1965).
[22] I. Grooms, K. Julien, J. B. Weiss, and E. Knobloch, Phys. Rev. Lett. **104**, 224501 (2010).
[23] K. Julien, E. Knobloch, and J. Werne, Theor. Comput. Fluid Dyn. **11**, 251 (1998).
[24] K. Julien, E. Knobloch, R. Milliff, and J. Werne, J. Fluid Mech. **555**, 233 (2006).
[25] K. Julien, S. Legg, J. McWilliams, and J. Werne, J. Fluid Mech. **322**, 243 (1996).
[26] J.-Q. Zhong, R. J. A. M. Stevens, H. J. H. Clercx, R. Verzicco, D. Lohse, and G. Ahlers, Phys. Rev. Lett. **102**, 044502 (2009).